Restoring Low Sidelobe Antenna Patterns with Failed Elements in a Phased Array Antenna

Steven I. Krich*, Life Member, IEEE, and Ian Weiner

***Abstract*—Maintaining low spatial sidelobes, despite the failure of individual antenna elements, is important for many radar and communication systems utilizing phased arrays. Techniques in the literature require accurate antenna element pattern data. In this paper we present a new algorithm for computing low-sidelobe beamforming which only requires the original beamforming weights which produce low sidelobes when all elements are functioning normally. The algorithm does not require accurate knowledge of the antenna element patterns, and permits user adjustment of the trade-off between sidelobe level, taper loss, and mainbeam width. Near optimum low sidelobes are demonstrated in several examples.**

***Index Terms* — Array signal processing, beams, linear algebra, phased arrays, shaped beam antennas.**

I. INTRODUCTION

For many phased array antenna applications, low spatial sidelobes are required, and it is desirable to maintain these low sidelobes despite the failure of one or more antenna elements. For most systems the array manifold (i.e., the individual complex antenna element patterns) are known well enough to compute a low spatial sidelobe pattern despite the failure of several elements, as described in [1-8]. For this paper it is assumed the low sidelobe beamformers with no failed elements are known. However with failed elements the array manifold is not known accurately enough to apply any of the referenced approaches. The complex antenna element patterns are different and the measurement errors are too large. Nothing has been found in the literature for this problem. The authors published a paper in ICASSP 2012 on this topic [9]. This expanded paper provides detailed mathematical justification, performance bounds, and additional techniques not included in the earlier paper.

Specifically, consider an n element phased array and the following length n vectors. Let $\boldsymbol{\theta}$ be an angular direction which for a two dimenstional array is a vector of length 2 and for a one dimentional array is a scalar. Let $\widetilde{\boldsymbol{\theta}}$ be the desired direction for a low sidelobe beamformer. We assume with no failed elements the following length n vectors are UNKNOWN and KNOWN and all vectors except for $\boldsymbol{\varepsilon}(\boldsymbol{\theta})$ are unit normed.

UNKNOWN for all $\boldsymbol{\theta}$

- $\boldsymbol{v}_t(\boldsymbol{\theta})$: true steering vector to angle $\boldsymbol{\theta}$ (i.e., on the array manifold)
- $\boldsymbol{\varepsilon}(\boldsymbol{\theta})$: antenna array manifold (calibration) errors

KNOWN

- $\boldsymbol{w}(\boldsymbol{\theta})$: low sidelobe beamformers for all $\boldsymbol{\theta}$ within a neighborhood around $\widetilde{\boldsymbol{\theta}}$, where the inner product $\langle \boldsymbol{w}(\boldsymbol{\theta}), \boldsymbol{v}_t(\boldsymbol{\theta}+\boldsymbol{\Delta})\rangle$ is small for $\boldsymbol{\theta}+\boldsymbol{\Delta}$ in the sidelobe region
- $\boldsymbol{v}_a(\widetilde{\boldsymbol{\theta}}) = [\boldsymbol{v}_t(\widetilde{\boldsymbol{\theta}}) + \boldsymbol{\varepsilon}(\widetilde{\boldsymbol{\theta}})] / \left|\boldsymbol{v}_t(\widetilde{\boldsymbol{\theta}}) + \boldsymbol{\varepsilon}(\widetilde{\boldsymbol{\theta}})\right|$: assumed steering vector to angle $\widetilde{\boldsymbol{\theta}}$

The foundation of this paper is the observation that with failed elements and perfect knowledge of the array manifold, a nearly optimal low sidelobe beamformer is represented by a linear combination of low sidelobe beamformers with no failed elements, $\boldsymbol{w}(\boldsymbol{\theta})$'s, in a neighborhood around $\widetilde{\boldsymbol{\theta}}$ under the constraint that the linear combination has zeros at the location of the failed elements. Furthermore since each of these low sidelobe beamformers achieve low sidelobes, we would expect that linear combinations of them in a neighborhood around $\widetilde{\boldsymbol{\theta}}$ would also have low sidelobes.

The algorithms in this paper exploit this observation using only the KNOWN vectors. The paper derives equations for estimating taper loss, sidelobe level, and mainbeam region width, and the algorithm permits optimization trade-offs among these three important criteria. Examples achieve a near optimal solution comparable to accurately knowing $\boldsymbol{v}_t(\boldsymbol{\theta})$ for all $\boldsymbol{\theta}$. Thus for some systems, in particular where a rapid recalculation of the beamformer with failed elements is required, it may be preferable to use this method even if $\boldsymbol{v}_t(\boldsymbol{\theta})$ is accurately known.

The reader may be wondering how the $\boldsymbol{w}(\boldsymbol{\theta})$'s could have been determined in the first place without knowing the array manifold. Examples are airborne radars that during low sidelobe antenna pattern calibration flights, form beams by minimizing the sidelobe ground clutter. The method in [10] iteratively adjusts the beamformer and only requires observability of the single beam. Space Time Adaptive Processing (STAP) [11] requires a fully digitized array. STAP could also be used with failed elements but may not be available during normal radar operation.

Distribution A: Public Release. This work is sponsored by the Department of the Air Force under Air Force contract #FA8721-05-C-0002. Opinions, interpretations, conclusions and recommendations are those of the authors and are not necessarily endorsed by the United States Government.

*S. I. Krich is withMassachusetts Institute of Technology Lincoln Laboratory, Lexington, MA 02421 USA (e-mail: sik23@cornell.edu).

I. Weiner is with Harvard University, Cambridge, MA 02138 USA on leave from Lincoln Laboratory, Lexington, MA 02421 USA (e-mail: iweiner@seas.harvard.edu).

Depending upon the nature of the antenna element failure, the mutual coupling between elements can change, which impacts the true array manifold. The results here and [1-8] apply to cases in which these changes are small. For example, failures that do not change the impedance at the antenna port have a negligible effect upon the mutual coupling.

Section II describes methods for recomputing the beamformer weights with failed elements. Section III provides examples for both one- and two-dimensional arrays. Section IV applies these techniques to arrays with no failed elements to modify either the taper loss or the sidelobe level. It is common for techniques developed for phased antenna arrays to also be applicable in the temporal domain and thus Section V discusses how the same technique is applicable for pulse-Doppler radars with missing pulses or missing range samples due to interference. Section VI is a summary.

II. Failed Element Algorithm

Fig. 1 shows a digitally controlled beamformer, $\boldsymbol{w}(\tilde{\boldsymbol{\theta}})$, applied to the $\boldsymbol{n}$ element array to produce a single beam. If elements are digitized the beamformer is digital; otherwise it is analog.

A. Beamformer with good antenna calibration

We start by describing a procedure which could be used with good knowledge of the array manifold. With no failed elements, we could compute a low sidelobe beamformer $\hat{\boldsymbol{w}}(\tilde{\boldsymbol{\theta}})$ by modeling a covariance matrix with sidelobe interference.

$$\hat{\boldsymbol{w}}(\tilde{\boldsymbol{\theta}}) = \mu[\gamma I + (1-\gamma)M(\tilde{\boldsymbol{\theta}})]^{-1}\boldsymbol{v}_a(\tilde{\boldsymbol{\theta}})$$
$$M(\tilde{\boldsymbol{\theta}}) = \frac{1}{L}\sum_{\theta_i\,\varepsilon\,\Omega_{SL}} \boldsymbol{v_a}(\boldsymbol{\theta}_i)\boldsymbol{v_a}(\boldsymbol{\theta}_i)^H \quad . \tag{1}$$

where I is an identiy matrix representing the thermal noise, $M(\tilde{\boldsymbol{\theta}})$ is the modeled sidelobe interference covariance matrix with no noise, γ controls the mixture of modeled interference to thermal noise, Ω_{SL} is the set of sidelobe directions, L is the number of terms in the sum, μ is a normalizing scale factor, and H is Hermitian transpose. With failed elements, the corresponding rows and columns of vectors and matrices are deleted. With very good knowledge of the array manifold, this procedure works very well but unfortunately with or without failed elements, the procedure will fail to achieve low sidelobes if the array manifold errors are too large.

Using just the KNOWN quantities in Section I, the next three sections derive procedures for selecting the number of $\boldsymbol{w}(\boldsymbol{\theta})$'s to include in this linear combination, their relative weighting, plus estimates for the resulting sidelobe level achieved and the taper loss. The ability to estimate sidelobe level and taper loss permits optimization trades.

B. Beamformer with constraints

Here we modify (1) by constraining the solution to a specific subspace. Let W_K be a matrix whose columns are K low sidelobe beamformers surrounding the direction $\tilde{\boldsymbol{\theta}}$ of interest. These should be closely spaced (less than a beamwidth) and preferably include $\boldsymbol{w}(\tilde{\boldsymbol{\theta}})$ as a column. We constrain the solution to the vector space spanned by W_K as follows. Let $J < K$ be the number of failed elements and $\boldsymbol{D} = [d_1, d_2, \ldots, d_J]^T$ be a vector for the locations of the failed elements. Within the space spanned by W_K is a subspace S of dimension $K-J$ where all vectors in S have a 0 at the locations of the failed elements. We compute this subspace as follows. Using MATLAB notation, $W_K(\boldsymbol{D},:)$ is a $J \times K$ matrix of only the rows of W_K with failed elements. The $K \times K-J$ matrix

$$Z = \mathrm{null}\big(W_K(\boldsymbol{D},:)\big) \tag{2}$$

is an orthonormal basis for the null space of $W_K(\boldsymbol{D},:)$ obtained from the singular value decomposition. That is, $W_K(\boldsymbol{D},:)Z$ is a $J \times (K-J)$ matrix of 0s and thus $W_K Z$ is an $n \times (K-J)$ matrix with 0s along the rows corresponding to the location of the J failed elements. We constrain the solution to subspace S thereby modifying (1) as follows

$$\begin{aligned}\tilde{\boldsymbol{w}}(\tilde{\boldsymbol{\theta}}) &= \mu W_K Z\big[(W_K Z)^H[\gamma I + (1-\gamma)M(\tilde{\theta})](W_K Z)\big]^{-1}(W_K Z)^H \boldsymbol{v}_a(\tilde{\boldsymbol{\theta}}) \\ &= \mu W_K Z\big[\gamma Z^H W_K^H W_K Z + (1-\gamma)Z^H G(\tilde{\theta})Z\big]^{-1}(W_K Z)^H \boldsymbol{v}_a(\tilde{\boldsymbol{\theta}})\end{aligned} \tag{3}$$

where

$$G(\tilde{\boldsymbol{\theta}}) = W_K^H M(\tilde{\boldsymbol{\theta}}) W_K \, . \tag{4}$$

The next two sections develop different approximations to $G(\tilde{\boldsymbol{\theta}})$ based upon different assumptions on how the low sidelobe beamformers, $\boldsymbol{w}(\boldsymbol{\theta})$'s, were formed.

C. Uncorrelated beam approximation to G

We never actually compute $M(\tilde{\boldsymbol{\theta}})$ but it is helpful to think of Ω_{SL} as the sidelobe region which is outside the mainlobe of all the beamformers in W_K. From (1) and (4) we can write

$$G(\tilde{\boldsymbol{\theta}}) = \frac{1}{L}\sum_{\theta_i\,\varepsilon\,\Omega_{SL}} [W_K^H \boldsymbol{v}_a(\boldsymbol{\theta}_i)][\boldsymbol{v}_a(\boldsymbol{\theta}_i)^H W_K] \quad . \tag{5}$$

where $W_K^H \boldsymbol{v}_t(\boldsymbol{\theta}_i)$ is a vector for the sidelobe level at $\boldsymbol{\theta}_i$ for each of the K beamformers in W_K. We assume now that the process by which all of the beamformers in W_K were produced yield the same average sidelobe level α, but the actual sidelobes averaged over Ω_{SL} are approximately uncorrelated from beam to beam. For example if $\boldsymbol{w}(\boldsymbol{\theta}) = \ddot{\boldsymbol{w}}(\boldsymbol{\theta}) + \boldsymbol{x}(\boldsymbol{\theta})$ where $\ddot{\boldsymbol{w}}(\boldsymbol{\theta})$ has lower sidelobes than $\boldsymbol{w}(\boldsymbol{\theta})$ and the sidelobe level is established by random vector $\boldsymbol{x}(\boldsymbol{\theta})$ which is different for each $\boldsymbol{\theta}$. Thus due to the averaging over the sidelobe angles, the off diagonal terms in (5) are small and can be approximated as zero. Our assumption yields the approximation

$$G_1(\tilde{\boldsymbol{\theta}}) = \alpha I \, . \tag{6}$$

D. Covariance estimate to G

Any small angle dependent variations in the element antenna patterns from element to element will impose a fundamental

minimum on the level of antenna sidelobes that can be achieved. Here we consider the case where the $\boldsymbol{w}(\boldsymbol{\theta})$'s are close to this limit with small taper loss as, for example, if they were generated using (1) with $\gamma = 0$ with excellent knowledge of the array manifold.

Under the conditions described, the original beamformer $\boldsymbol{w}(\tilde{\boldsymbol{\theta}})$ is close to optimal with respect to $G(\tilde{\boldsymbol{\theta}})$, so it is reasonable to seek an approximation $G_2(\tilde{\boldsymbol{\theta}})$ which preserves this property; This can be expressed via covariance inversion, or by the equivalent requirement that $G_2(\tilde{\boldsymbol{\theta}})\boldsymbol{w}(\tilde{\boldsymbol{\theta}}) \propto \boldsymbol{v}_a(\tilde{\boldsymbol{\theta}})$. In addition, similarly to G_1 above, we require that sidelobe estimates for each of the $\boldsymbol{w}_k$ agree with observation [see (9) below].

A straightforward computation shows that the following (positive-definite, Hermitian) matrix satisfies these two key model requirements:

$$G_2(\tilde{\boldsymbol{\theta}}) = \alpha\left[\frac{1}{\left|\boldsymbol{v}_a(\tilde{\boldsymbol{\theta}})^H \boldsymbol{w}(\tilde{\boldsymbol{\theta}})\right|^2} W_K^H \boldsymbol{v}_a(\tilde{\boldsymbol{\theta}})\boldsymbol{v}_a(\tilde{\boldsymbol{\theta}})^H W_K + \operatorname{diag}\left(1 - \frac{\left|\boldsymbol{v}_a(\tilde{\boldsymbol{\theta}})^H \boldsymbol{w}_k\right|^2}{\left|\boldsymbol{v}_a(\tilde{\boldsymbol{\theta}})^H \boldsymbol{w}(\tilde{\boldsymbol{\theta}})\right|^2}\right)\right] \tag{7}$$

where $\boldsymbol{w}_k$, $k = 1,2,\ldots K$ are the chosen beamformers which form the columns of W_K, and the MATLAB notation for a diagonal matrix is being used.

E. Taper loss and sidelobe estimate

In choosing parameters K and γ it is important to have an estimate for the taper loss and changes in the average sidelobes. The taper loss estimate is

$$TL\left(\tilde{\boldsymbol{w}}(\tilde{\boldsymbol{\theta}})\right) = \left|\tilde{\boldsymbol{w}}(\tilde{\boldsymbol{\theta}})^H \boldsymbol{v}_a(\tilde{\boldsymbol{\theta}})\right|^2 \leq 1 \tag{8}$$

where $\tilde{\boldsymbol{w}}(\tilde{\boldsymbol{\theta}})$ and $\boldsymbol{v}_a(\tilde{\boldsymbol{\theta}})$ are unit normed. The manifold errors may be too large to achieve the desired sidelobes using the methods in [1-8]; however, this taper loss estimate is quite accurate unless the manifold errors are very large.

We can write $\tilde{\boldsymbol{w}}(\tilde{\boldsymbol{\theta}}) = W_K\hat{\boldsymbol{c}}$ where $\hat{\boldsymbol{c}}$ is determined from (3). Since $M(\tilde{\boldsymbol{\theta}})$ is a covariance matrix of steering vectors in the sidelobe region, the average sidelobes is

$$\begin{aligned} SL\left(\tilde{\boldsymbol{w}}(\tilde{\boldsymbol{\theta}})\right) &= \tilde{\boldsymbol{w}}(\tilde{\boldsymbol{\theta}})^H M(\tilde{\boldsymbol{\theta}})\tilde{\boldsymbol{w}}(\tilde{\boldsymbol{\theta}}) \\ &= \hat{\boldsymbol{c}}^H W_K^H M(\tilde{\boldsymbol{\theta}}) W_K \hat{\boldsymbol{c}} \\ &= \hat{\boldsymbol{c}}^H G(\tilde{\boldsymbol{\theta}})\hat{\boldsymbol{c}} \ . \end{aligned} \tag{9}$$

Using the approximation $G_i(\tilde{\boldsymbol{\theta}})$ in (6) or (7) in place of $G(\tilde{\boldsymbol{\theta}})$, we estimate the change of sidelobes as

$$\Delta SL_{est}\left(\tilde{\boldsymbol{w}}(\tilde{\boldsymbol{\theta}})\right) = \frac{\hat{\boldsymbol{c}}^H G_i(\tilde{\boldsymbol{\theta}})\hat{\boldsymbol{c}}}{\alpha} \quad i = 1 \text{ or } 2\,. \tag{10}$$

One does not need to know the value for α to use (10) since by the way $G_i(\tilde{\boldsymbol{\theta}})$ is defined in (6) or (7) α cancels. The appendix develops some rough upper bounds on the error incurred by using $G_i(\tilde{\boldsymbol{\theta}})$. For small enough perturbations from the original vector, (9) gives a good approximation even if (6) or (7) are not uniformly good approximations to $G(\tilde{\boldsymbol{\theta}})$.

F. Choosing parameters K and γ

In (3) γ controls the mixture of modeled interference to thermal noise. For $\gamma = 1$ this is a projection of $\boldsymbol{v}_a(\tilde{\boldsymbol{\theta}})$ onto the space spanned by the columns of $W_K Z$ and thus has the best taper loss but the highest estimated sidelobes. As γ decreases, the taper loss monotonically degrades and the estimated sidelobe power monotonically improves. (See, for example, theorem II in [12].) $\gamma < 1$ has the effect of regularizing the matrix $Z^H W_K^H W_K Z$ by reducing the contribution of the eigenvectors corresponding to its small eigenvalues. These monotonicity properties are very useful for choosing parameters in the optimization procedures below.

As is always the case when choosing beamforming weights, trade-offs can be made between taper loss, sidelobe level, and mainbeam region. Therefore, parameter choices must be determined in part by the properties most important to the application. However, the choice is simplified greatly by the monotonicity observations above. *K* directly impacts the width of the mainbeam region. Under our correction scheme, the coefficients of the linear combination of neighboring beams are roughly the corrected pattern gain at their corresponding look directions. Therefore a larger *K* will create a wider mainbeam region manifested as some combination of a wider mainlobe and/or high first sidelobes. Note that, even with antenna manifold errors, the shape of this resultant mainbeam region can be predicted and possibly adjusted depending on the needs of the application. No matter which method is chosen to estimate $G(\tilde{\boldsymbol{\theta}})$, two procedures follow depending upon the desired goals. For both procedures it is convenient to take $\alpha = 1$ since we only estimate the change in the sidelobe levels in (10) and the actual sidelobe levels may be unknown.

In Procedure 1 we set a goal for the change in the average sidelobes, ΔSL_{goal}, to achieve and a bound on the taper loss, $\mathrm{TL}_{\mathrm{bound}}$ to avoid exceeding. These are estimated using (8) and (10). It is usually impossible to achieve both of these exactly. Procedure 2 is the reverse with a bound on the change in average sidelobes, ΔSL_{bound}, and a goal for the taper loss, TL_{goal}.

Procedure 1 is flow charted in Fig. 2 in which values for *K* and γ are found such that $\Delta SL_{est}(\tilde{\boldsymbol{w}}) = \Delta SL_{goal}$ and the taper loss, $TL(\tilde{\boldsymbol{w}})$, is lower bounded by $\mathrm{TL}_{\mathrm{bound}}$. (Note: $\Delta SL_{goal} = 1$ means unchanged sidelobes and $TL(\tilde{\boldsymbol{w}})$ is negative.) Finding γ in the interval [0,1] is simplified by the monotonicity discussed above for the function in (8). *K* is increased until an acceptable criteria are met.

Procedure 2 is flow charted in Fig. 3 in which taper loss $TL(\tilde{\boldsymbol{w}}) = TL_{goal}$ and $\Delta SL_{est}(\tilde{\boldsymbol{w}}) \leq \Delta SL_{bound}$. Here again *K* is increased until an acceptable criteria are met.

With either procedure, should the goal and bound requirements be too stringent to achieve, *K* will continue to increase to an unacceptably large value and a solution may not be found, in which case the goal and bound should be reset and the procedure repeated. *K* is constrained to be odd to

provide symmetric beams around the beam of interest though an odd value is not an inherent requirement.

III. Examples

A. 64 element uniform linear array with half wavelength spacing

The authors feel it is important that the validity of algorithms such as the one described in this paper be tested under real-world conditions. Specifically, we test the procedure using a perfect uniform linear array as the assumed array manifold, $\boldsymbol{v}_a(\boldsymbol{\theta})$, but a true array manifold, $\boldsymbol{v}_t(\boldsymbol{\theta})$, having small perturbations from the perfect uniform linear array. The manifold errors, $\boldsymbol{\varepsilon}(\boldsymbol{\theta})$, limit the achievable beamformer sidelobes using (1) to -30 dB. However, the beamforming weight vectors, $\boldsymbol{w}(\boldsymbol{\theta})$, to achieve low sidelobes are available. The beams in W_K are spaced by a half beamwidth (i.e., $\sin(\theta_i) = i/n$).

The manifold errors, $\boldsymbol{\varepsilon}(\boldsymbol{\theta})$, are modeled as independent circularly Gaussian on each element of the array. Since on individual elements the errors are likely to be correlated with look direction, for a beamwidth change in look direction the errors are correlated by 0.98 on each element but independent from element to element. This is achieved by starting with an $n\,x\,m$ matrix of independent circular Gaussian random variables, where n is the size of the array and m is a large number of closely spaced angles spanning all angles. The rows of this matrix are passed through a low pass filter to achieve the 0.98 correlation at one beamwidth. For the selected parameters, this limits the maximum achievable sidelobes.

In Fig. 4 we examine element 15 failure in the 64 element uniform linear array. Plotted are the algorithm results, the original with no failed elements, the original with element 15 set to 0, plus an optimum explained below. We used beamformer antenna patterns with the lowest possible sidelobes due to the element pattern differences from element to element and thus use $G_2(\widetilde{\boldsymbol{\theta}})$ with procedure 1, $\Delta SL_{goal} = 0$ dB (i.e., unchanged sidelobes) and $TL_{bound} = -3.2\ dB$. The relevant parameters K, γ, and taper loss are indicated. The mainlobe is a little wider but the sidelobes are about the same as the pattern with no failed elements.

In order to evaluate the performance of the correction algorithm, we include in Fig. 4 a comparison with an optimum approach. We define the optimum beamformer as the one resulting from (1) with no manifold errors and γ selected to maintain unchanged sidelobes and 2Δ chosen to be the angular width of the K beams in the algorithm. Notice that the algorithm and optimum patterns virtually overlay with identical taper losses. The (A11) bounds true sidelobes at 5.3 dB above the estimation, although the actual discrepancy between truth and estimation is less than 1 dB.

Fig. 5 repeats the previous example except the original sidelobe levels have been raised by 5 dB by adding a random vector and thus we use $G_1(\widetilde{\boldsymbol{\theta}})$. Here again, the algorithm and the optimum are virtually identical with similar taper losses. The (A2) bounds true sidelobes at 4.7 dB above the estimate but again the actual discrepancy is less.

Fig. 6 is the same as Fig. 4 except with three failed elements 15, 32, 53. Here again the optimum and the algorithm agree well. The high first sidelobes are primarily due to deleting an element in the middle of the array. Had we plotted results for the single element 32 failure, a similar high first sidelobe appears. The bound given by (A11) is 8.3 dB which is not very tight due to the large value of K.

Fig. 7 shows the amplitudes of each component of $\widetilde{\boldsymbol{w}}(\widetilde{\boldsymbol{\theta}})$ from Figs. 4 and 6 for both the algorithm and optimum which are very similar. The jagged nature is due to the modeling of the antenna element errors. In all cases maximum use is made of the largest contiguous interval of operating elements.

Fig. 8 repeats Fig. 5 except we choose parameters to reduce the taper loss by allowing for higher sidelobes. We apply procedure 2 and set $TL_{goal} = 2.5\ dB$ and $\Delta SL_{bound} = 1\ dB$. The actual achieved change in sidelobes was $1.6\ dB$. The reduction in the taper loss resulted in high first sidelobes. Here (A2) bounds true sidelobes at 8.9 dB above the estimate.

These examples demonstrate the ability to trade sidelobes for lower taper loss.

B. Two-dimensional array examples

Here we show the application of the algorithm to a two-dimensional array. The array errors were modeled in the same way as the one-dimensional example with errors correlated in both dimensions. Fig. 9 shows a low sidelobe pattern for a 16 x 16 element array having sidelobe levels of -52 dB off the cardinal axis and -39 dB on the cardinal axis. Figs. 10 and 11 show the patterns with two failed elements at coordinates [4,8] and [8,12] before and after correction where the goal was to match the original sidelobe levels. Here we chose procedure 1, $G_1(\widetilde{\boldsymbol{\theta}})$, and a two-dimensional grid of beams spaced by half beamwidth. The criteria were met with $K = 13$ and $\gamma = 0.43$. Figs. 12 and 13 show the beamformer amplitudes applied to each element before and after correction where the jagged nature is due to the nature of the antenna manifold errors. Notice in Fig. 13 the algorithm places emphasis on the elements in the upper right-hand corner to take advantage of the largest contiguous area of operating elements. The optimum approach does similarly. The achieved sidelobes in Fig. 11 are unchanged off the cardinal axis but are raised 2 dB on the cardinal axis. The taper loss has increased from -1.8 dB to -3.0 dB. Better taper losses are achievable with larger values of K. For example with $K = 25$ it is possible to achieve a taper loss of -1.9 dB, comparable sidelobe levels, but higher near in sidelobes.

IV. Sidelobe Adjustments with no failed elements

For some applications it may be desirable to dynamically control the taper loss or sidelobe level with no failed elements. Fig.14 shows results using procedure 2 where the taper loss has been reduced by 0.9 dB. The pattern has high first sidelobes, near in sidelobes have been raised and far out sidelobes are about the same. Different values of K and γ yield different changes to the pattern.

V. Pulse-Doppler radar application

As is frequently the case, techniques developed in either the spatial or the temporal domain frequently finds application in the other domain. Consider a pulse-Doppler radar in which

one or more pulses are severely interfered with, but low Doppler sidelobes are needed with these pulses dropped. Mathematically, the missing pulses replace the failed elements, and the Doppler filters replace the low sidelobe beamformers. The techniques in this paper offer a rapid and predicable outcome for taper losses and Doppler sidelobe level. Since here manifold errors are likely not to be an issue, it may be preferable to use (3) instead of the approximation in (7) for the covariance matrix. Furthermore, the techniques in [1-8] are also applicable but may be more computationally intense with little added benefit.

Similarly temporal samples in the range domain may be interfered with and low range sidelobes are needed even with these dropped samples. Mathematically the pulse compression filter replaces the low sidelobe beamformers.

VI. Summary

We started with the observation that a low sidelobe beamformer with failed elements could be formed by a linear combination of a few beamformers around the direction of interest constrained to have a 0 at the location of the failed elements. To choose the number of beamformers, K, and the relative value of modeled thermal noise, γ, we derived an approximation for the change in sidelobe level and the taper loss. We have thus demonstrated a robust method for calculating a low sidelobe beamformer with failed elements where we can control the achieved sidelobe levels, the taper loss, or the width of the mainbeam region.

The approach is also applicable to forming beams with no failed elements to reduce taper losses by raising the sidelobes. Also discussed was the application of the algorithm in pulse-Doppler radars for missing pulses or missing range samples with the goal of maintaining low Doppler or range sidelobes.

The method has been shown to be near optimal and thus may find application even for systems with good knowledge of the antenna manifold.

Appendix

Here we examine the two variations of the sidelobe estimator and derive bounds on how much they can underestimate the true sidelobe levels.

Ideally we would like perfect agreement of estimation with truth. This is impossible without detailed measurements, but for a good choice of G_{est} we can at least avoid the unacceptable situation of choosing a beamforming weight vector for which $SL_{est}(\boldsymbol{c}) \ll SL_{true}(\boldsymbol{c})$.

While the results can be generalized, for simplicity we assume here that sidelobes of all the beams $\boldsymbol{w}_k$ are all approximately equal to α. All $\boldsymbol{w}$ vectors in this appendix are constructed from the columns of the W_K matrix, and so each such $\boldsymbol{w}$ uniquely defines a corresponding $\boldsymbol{c} \in \mathbb{C}^K$ by the equation $\boldsymbol{w} = W_K\boldsymbol{c}$, or equivalently, $\boldsymbol{c} = (W_K^H W_K)^{-1} W_K^H \boldsymbol{w}$. We define the vectors $\boldsymbol{e}_k$ by $\boldsymbol{w}_k = W_K \boldsymbol{e}_k$; Thus $\boldsymbol{e}_k$ is simply the k^{th} standard basis vector of $\mathbb{C}^K$, that is, a vector with a 1 in the k^{th} position and 0 elsewhere. For convenience, we let the index k vary from $-\frac{K-1}{2}$ to $+\frac{K-1}{2}$. Since the look direction of interest, $\boldsymbol{\theta}$, is fixed, we use the simplified notation, $\boldsymbol{w}_0 = \boldsymbol{w}(\boldsymbol{\theta})$, and $\boldsymbol{e}_0 = (W_K^H W_K)^{-1} W_K^H \boldsymbol{w}_0$. We use the notation $\boldsymbol{q}_a = W_K^H \boldsymbol{v}_a$ to represent the constraint vector in the W_K beamspace. When we refer to taper loss in this appendix, we always mean with respect to the assumed steering vector, which for the purposes of this paper should be nearly indistinguishable from the true (unmeasurable) taper loss. We remind the reader that M, hence also G, is formed by excluding a mainbeam guard region wide enough to exclude the mainbeam regions of all the beams in W. Let G_{est} be the model covariance matrix used in sidelobe estimation, in the beamspace basis.

The bounds will make use of the following well-known inequality: If $a_1, a_2, \ldots, a_K$ are real numbers, then

$$(a_1 + \cdots + a_K)^2 \le K \cdot (a_1^2 + \cdots + a_K^2) \tag{A1}$$

This inequality may be proven several ways. For example, one can multiply out the terms on the left-hand side of (A1) and repeatedly apply the simpler inequality $2a_i a_j \le a_i^2 + a_j^2$, which follows easily from $(a_i - a_j)^2 \ge 0$.

A. Diagonal Model Covariance Matrix

Let α_k denote the sidelobe power levels of the beamformer $\boldsymbol{w}_k$, and define $G_{est} = \mathrm{diag}(\alpha_k)$. If we are estimating the sidelobes of $\boldsymbol{w} = W_K\boldsymbol{c}$, and $\boldsymbol{c} = \sum c_k \boldsymbol{e}_k$, then the highest possible sidelobes occur when the terms in the sum add in phase:

$$SL_{true}(\boldsymbol{c}) \le \left(\sum |c_k| \cdot |\alpha_k|^{1/2}\right)^2 \tag{A2}$$

One can directly apply (A2) to compute a worst-case bound on sidelobes of a $\hat{\boldsymbol{c}}$ obtained from one of the algorithms in this paper. In general, applying (A1) to the sum yields

$$\frac{SL_{true}(\boldsymbol{c})}{SL_{est}(\boldsymbol{c})} \le \frac{\left(\sum |c_k| \cdot |\alpha_k|^{1/2}\right)^2}{\sum |c_k|^2 \, \alpha_k} \le K \tag{A3}$$

so that, for small values of K, estimation error is acceptably low. Of course, estimates of average sidelobe levels in any spatial region of interest, as well as peak sidelobe estimates, can be bounded in a similar manner.

In the body of the paper (6) assumes the special case in which $\alpha_k \equiv \alpha$ is independent of k. Examples using (6) apply this bound.

B. Model Covariance Matrix For $\boldsymbol{w}_0$ Optimal

Here we follow the definition from Section II.D. We will considerably simplify our computations with the following additional notation: $TL_k \equiv |\boldsymbol{q}_a^H \boldsymbol{e}_k|^2 = |\boldsymbol{v}_a^H \boldsymbol{w}_k|^2$ is the taper loss for the k^{th} beam, $\rho_k \equiv \boldsymbol{e}_k^H G \boldsymbol{e}_k / TL_k$, and $\Delta_{k,l} \equiv \rho_k - \rho_l$. We will sometimes also use $\|\boldsymbol{c}\|_G^2 \equiv \boldsymbol{c}^H G \boldsymbol{c}$.

Using our compressed notation:

$$G_{est} = \rho_0 \cdot \boldsymbol{q}_a \boldsymbol{q}_a^H + \mathrm{diag}\left(TL_k \cdot \Delta_{k,0}\right) \tag{A4}$$

It can easily be verified that G_{est} has the following desirable properties: 1) G_{est} is a positive-definite, Hermitian matrix, 2) $\boldsymbol{e}_k^H G_{est} \boldsymbol{e}_k = \boldsymbol{e}_k^H G \boldsymbol{e}_k$ for all k, and 3) $G_{est}\boldsymbol{e}_0 = (\alpha / \boldsymbol{e}_0^H \boldsymbol{q}_a)\boldsymbol{q}_a$.

The first is a requirement for a sensible model covariance matrix. The second says that G_{est} agrees with G on the basis vectors (known from observation). The third says that $\boldsymbol{e}_0 \propto G_{est}^{-1}(\boldsymbol{q}_a)$, that is, our original weight vector $\boldsymbol{e}_0$ can be obtained by covariance matrix inversion using G_{est} in the W_K beamspace, thus G_{est} is a model covariance matrix for which $\boldsymbol{w}_0$ is optimal.

Now we bound the error incurred by this approximation. Denote by $\boldsymbol{w}_{opt} = W_K \boldsymbol{c}_{opt}$ the true unit-normed optimal under M when restricted to the W_K beamspace, so that $G\boldsymbol{c}_{opt} \propto \boldsymbol{q}_a$. Let $TL_{opt} = \left|\boldsymbol{q}_a^H \boldsymbol{c}_{opt}\right|^2$ be the taper loss of the true optimal, and similarly define ρ_{opt} and $\Delta_{k,opt}$.

We will use the following shortly: If $\boldsymbol{x}$ is any vector such that $\boldsymbol{q}_a^H \boldsymbol{x} = 0$, we have

$$\boldsymbol{c}_{opt}^H G \boldsymbol{x} = \left(G\boldsymbol{c}_{opt}\right)^H \boldsymbol{x} \propto \boldsymbol{q}_a^H \boldsymbol{x} = 0 \tag{A5}$$

Define vectors $\boldsymbol{\tau}_k$ and $\boldsymbol{\delta}_k$ by

$$\begin{aligned} \boldsymbol{\tau}_k &= \boldsymbol{e}_k - \frac{\boldsymbol{q}_a^H \boldsymbol{e}_k}{\boldsymbol{q}_a^H \boldsymbol{c}_{opt}} \boldsymbol{c}_{opt} \\ \boldsymbol{\delta}_k &= \boldsymbol{e}_k - \frac{\boldsymbol{q}_a^H \boldsymbol{e}_k}{\boldsymbol{q}_a^H \boldsymbol{e}_0} \boldsymbol{e}_0 \end{aligned} \tag{A6}$$

By these definitions one can easily verify that, for all k,

$$\begin{aligned} \boldsymbol{q}_a^H \boldsymbol{\tau}_k = 0 = \boldsymbol{q}_a^H \boldsymbol{\delta}_k \\ \boldsymbol{\delta}_k = \boldsymbol{\tau}_k - \frac{\boldsymbol{q}_a^H \boldsymbol{e}_k}{\boldsymbol{q}_a^H \boldsymbol{e}_0} \boldsymbol{\tau}_0 \end{aligned} \tag{A7}$$

We will need the following, which is computed using (A5), (A6), and (A7):

$$\|\boldsymbol{\tau}_k\|_G^2 = TL_k \cdot \Delta_{k,opt} \tag{A8}$$

Using (A7) and (A8) we get the following bound, which we will use shortly:

$$\begin{aligned} \|\boldsymbol{\delta}_k\|_G^2 &= \left\| \boldsymbol{\tau}_k - \frac{\boldsymbol{q}_a^H \boldsymbol{e}_k}{\boldsymbol{q}_a^H \boldsymbol{e}_0} \boldsymbol{\tau}_0 \right\|_G^2 \\ &\leq TL_k \cdot \left(\Delta_{k,opt} + \Delta_{0,opt} + 2\Delta_{0,opt}^{1/2} \Delta_{k,opt}^{1/2}\right) \end{aligned} \tag{A9}$$

Now we are ready to bound $\frac{\boldsymbol{c}^H G \boldsymbol{c}}{\boldsymbol{c}^H G_{est} \boldsymbol{c}}$ by expressing $\boldsymbol{c}$ in the $\{\boldsymbol{e}_0, \boldsymbol{\delta}_k\}_{k \neq 0}$ basis. We write:

$$\boldsymbol{c} = \left(\frac{\boldsymbol{q}_a^H \boldsymbol{c}}{\boldsymbol{q}_a^H \boldsymbol{e}_0}\right) \boldsymbol{e}_0 + \sum_{k \neq 0} c_k \boldsymbol{\delta}_k \tag{A10}$$

where $c_k = \boldsymbol{e}_k^H \boldsymbol{c}$ is simply the k^{th} component of $\boldsymbol{c}$ in the standard basis. To bound $\|\boldsymbol{c}\|_G^2 \equiv \boldsymbol{c}^H G \boldsymbol{c}$ we will use (A5)-(A8) and (A10), obtaining

$$\begin{aligned} \|\boldsymbol{c}\|_G^2 &= \left\| \frac{\boldsymbol{q}_a^H \boldsymbol{c}}{\boldsymbol{q}_a^H \boldsymbol{c}_{opt}} \boldsymbol{c}_{opt} + \frac{\boldsymbol{q}_a^H \boldsymbol{c}}{\boldsymbol{q}_a^H \boldsymbol{e}_0} \boldsymbol{\tau}_0 + \sum_{k \neq 0} c_k \boldsymbol{\delta}_k \right\|_G^2 \\ &= TL_c \cdot \rho_{opt} + \left\| \frac{\boldsymbol{q}_a^H \boldsymbol{c}}{\boldsymbol{q}_a^H \boldsymbol{e}_0} \boldsymbol{\tau}_0 + \sum_{k \neq 0} c_k \boldsymbol{\delta}_k \right\|_G^2 \\ &\leq TL_c \cdot \rho_{opt} + \left(\left| \frac{\boldsymbol{q}_a^H \boldsymbol{c}}{\boldsymbol{q}_a^H \boldsymbol{e}_0} \right| \|\boldsymbol{\tau}_0\|_G + \sum_{k \neq 0} |c_k| \cdot \|\boldsymbol{\delta}_k\|_G \right)^2 \\ &\leq TL_c \cdot \rho_0 + \left(\sum_{k \neq 0} |c_k| \cdot \|\boldsymbol{\delta}_k\|_G \right)^2 + \\ &\quad + 2\left(TL_c \cdot \Delta_{0,opt}\right)^{1/2} \sum_{k \neq 0} |c_k| \cdot \|\boldsymbol{\delta}_k\|_G \end{aligned} \tag{A11}$$

It remains to estimate the sidelobes and taper loss of $\boldsymbol{w}_{opt}$. In the primary case of interest, average sidelobes cannot be significantly reduced from that of $\boldsymbol{w}_0$ due to antenna errors, so we take $\boldsymbol{c}_{opt}^H G \boldsymbol{c}_{opt} \approx \alpha_0$. For an approximation of taper loss, note that largest (best) possible value for TL_{opt} is achieved by orthogonal projection of the assumed steering vector $\boldsymbol{v}_a$ into the W_K subspace. This estimation is overkill, but typically adequate. Substituting these estimates into our previous definitions gives us:

$$\Delta_{k,opt} \approx \frac{\alpha_k}{TL_k} - \frac{\alpha_0}{\boldsymbol{v}_a^H W_K (W_K^H W_K)^{-1} W_K^H \boldsymbol{v}_a} \tag{A12}$$

Substituting (A12) and (A9) into (A11) allows us to compute a numerical bound on true sidelobes, and thus, bound the estimation error. In the examples when (7) is used this bound is computed.

We can derive a much simpler bound in the special limiting case that $\Delta_{0,opt} \ll \rho_0$. Applying (A1) to (A11) gives:

$$\begin{aligned} \|\boldsymbol{c}\|_G^2 &\leq TL_c \cdot \left(\rho_0 + \Delta_{0,opt}\right) + K \sum_{k \neq 0} |c_k|^2 \cdot \|\boldsymbol{\delta}_k\|_G^2 \\ &\lesssim TL_c \cdot \rho_0 + K \sum_{k \neq 0} |c_k|^2 \cdot \|\boldsymbol{\delta}_k\|_G^2 \end{aligned} \tag{A13}$$

When $\Delta_{0,opt} \ll \rho_0$ in this case it is typical to also have $\Delta_{0,opt} \ll \Delta_{k,opt}$ for $k \neq 0$, allowing us to approximate (A9) as $\|\boldsymbol{\delta}_k\|_G^2 \lesssim TL_k \cdot \Delta_{k,0}$, yielding

$$\boldsymbol{c}^H G \boldsymbol{c} \lesssim TL_c \cdot \rho_0 + K \sum_{k \neq 0} |c_k|^2 \cdot TL_k \cdot \Delta_{k,0} \tag{A14}$$

In comparison, our estimate (A4) gives

$$\boldsymbol{c}^H G_{est} \boldsymbol{c} = TL_c \cdot \rho_0 + \sum_{k \neq 0} |c_k|^2 \cdot TL_k \cdot \Delta_{k,0} \tag{A15}$$

Therefore in this case the bound may be approximated simply as:

$$\frac{\boldsymbol{c}^H G \boldsymbol{c}}{\boldsymbol{c}^H G_{est} \boldsymbol{c}} \lesssim 1 + (K-1)\left(1 - \frac{\sigma_c^{est}}{\sigma_0}\right) \qquad \text{(A16)}$$

where $\sigma_0 = \frac{TL_0}{\alpha_0}$ and $\sigma_c^{est} = \frac{TL(c)}{\boldsymbol{c}^H G_{est} \boldsymbol{c}}$.

REFERENCES

[1] W. P. Keizer, and H. Stark, "Element failure correction for a large monopulse phased array antenna with active amplitude weighting," IEEE Trans. Antennas and Propagation, vol. 55, No. 8, pp. 2211-2218, August 2007.

[2] M. H. Er, "Array pattern synthesis in the presence of element failure," Proceeding of the ISAP '92, Sapporo, Japan, pp. 9–12, 1992.

[3] K. M. Lee, and R. Chu, S. Liu, "A built-in performance monitoring/fault isolation and correction (PM/FIC) system for active phased array antennas," *IEEE Antennas and Propagation Society International Symposium* 1993, pp. 206–9, vol.1.

[4] S. Liu, "A fault correction technique for phased array antennas," *IEEE Antennas and Propagation Society International Symposium 1992 Digest.* Publication Date: URSI Radio Science Meeting and Nuclear EMP Meeting, 1612–15, vol.3, 1992.

[5] T. J. Peters, "A conjugate gradient-based algorithm to minimize the sidelobe level of planar arrays with element failures," IEEE Trans. Antennas and Propagation, vol. 39, No.10, pp. 1497–1504, October 1991.

[6] P. J. Wright and D. Brandwood, "Re-optimisation of linear and planar arrays with failed elements," Ninth International Conference on Antennas and Propagation, pp. 81–84, vol.1, 1995.

[7] S.H. Zainud-Deen, M. Ibrahem, H. Sarshar, and S. Ibrahem, "Array failure correction with orthogonal method," 21st National Radio Conference (NRSC2004) (NTI), March 2004.

[8] Y. Yang, "Design of self-healing arrays using vector-space projections," IEEE Trans. Antennas and Propagation, Vol. 49, No. 4, pp. 526-534, April 2001.

[9] S. I. Krich, I. Weiner, and C. J. Prust "Low sidelobe antenna patterns with failed elements," ICASSP 2012 proceedings, Kyoto Japan.

[10] S. I. Krich, I. Weiner "Low-Sidelobe Antenna Beamforming Via Stochastic Optimization," IEEE Trans. Antennas and Propagation, vol. 62, No. 12, December 2014.

[11] R. Klemm, *Space-Time Adaptive Processing Principles and Applications.* London: Institute of Electrical Engineers, 1998.

[12] E. N. Gilbert and S. P. Morgan, "Optimum Design of Directive Antenna Arrays Subject to Random Variations," The Bell System Technical Journal, pp. 637-663, May 1955.

Steven I. Krich (M'71) received his BS, MS, and Ph.D. in electrical engineering (information theory) at Cornell University in 1966, 1968, and 1972, respectively.

Since 1972 he has been a researcher at MIT Lincoln Laboratory in Lexington MA investigating signal processing for radar and communication systems. His current research interests are adaptive signal processing for interference suppression with phased array antennas.

Ian Weiner received his BS degree in mathematics at Harvey Mudd College in 2001 and his MS in mathematics at Stanford University in 2009.

Since 2009 he has been a staff member of the Air Defense Techniques group at MIT Lincoln Laboratory. He is currently a doctoral candidate in applied mathematics at Harvard University. His research interests include signal processing, information theory, and differential geometry.

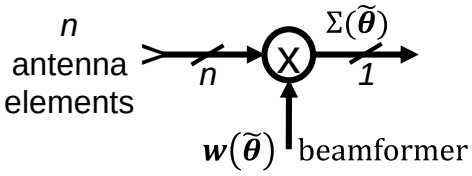

Fig. 1. Beamformer block diagram.

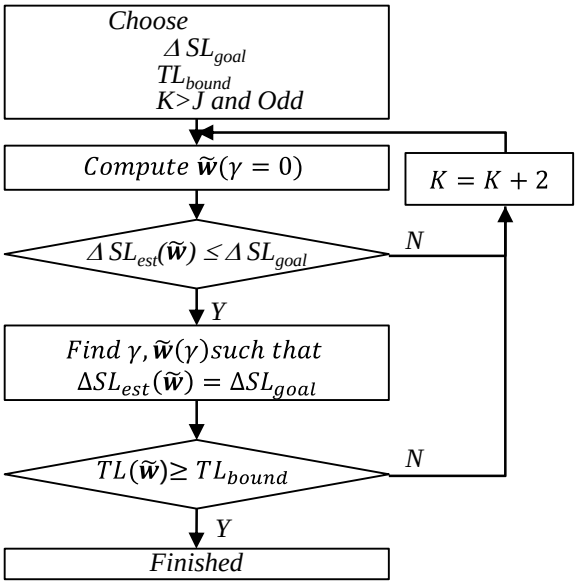

Fig. 2. Procedure for setting a goal for sidelobes and bound on taper loss.

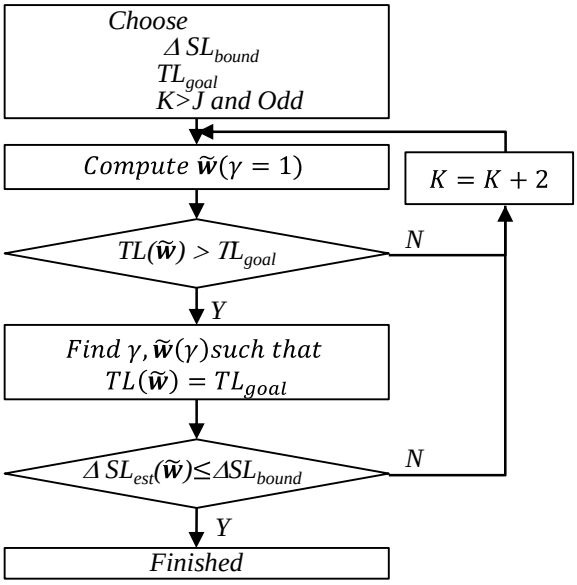

Fig. 3. Procedure for setting a goal for taper loss and a bound on sidelobes.

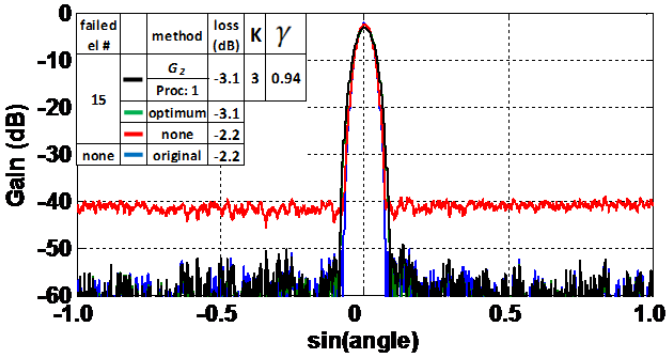

Fig. 4. Antenna patterns with failed element 15 with $\boldsymbol{G_2(\tilde{\theta})}$.

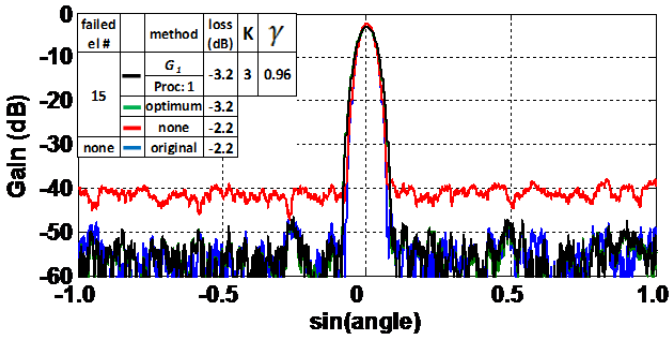

Fig. 5. Antenna patterns with failed element 15 with $\boldsymbol{G_1(\tilde{\theta})}$.

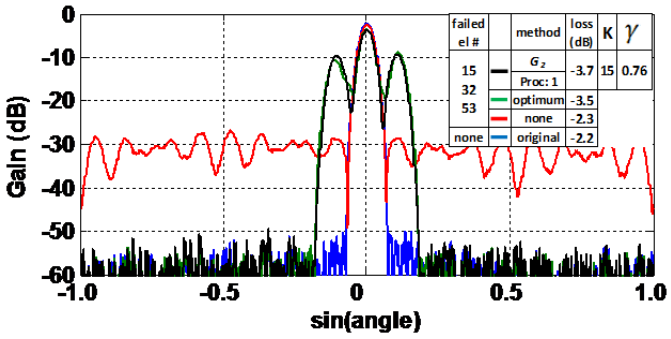

Fig. 6. Antenna patterns with failed elements 15, 32, and 53 with $\boldsymbol{G_2(\tilde{\theta})}$.

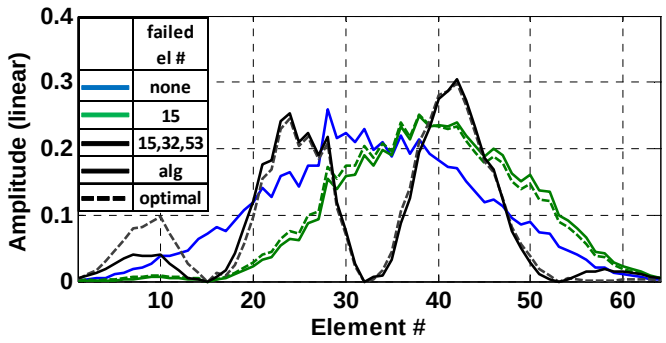

Fig. 7. Weight vector amplitudes for cases in Figs. 5 and 7.

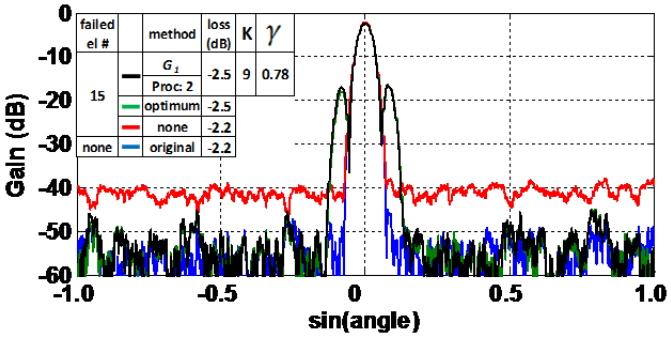

Fig. 8. Antenna patterns with taper loss limited to -2.5 dB.

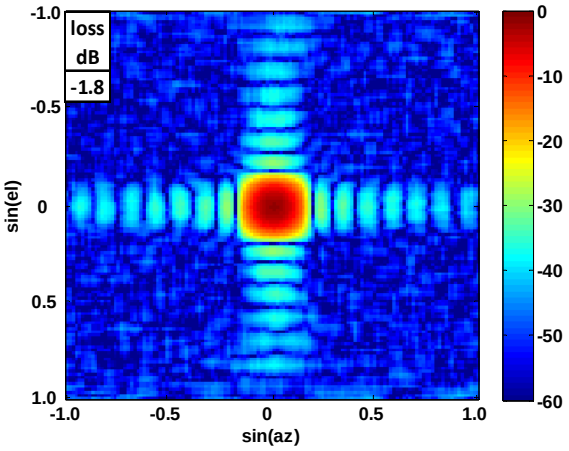

Fig. 9. Low sidelobe pattern for 16 x 16 array.

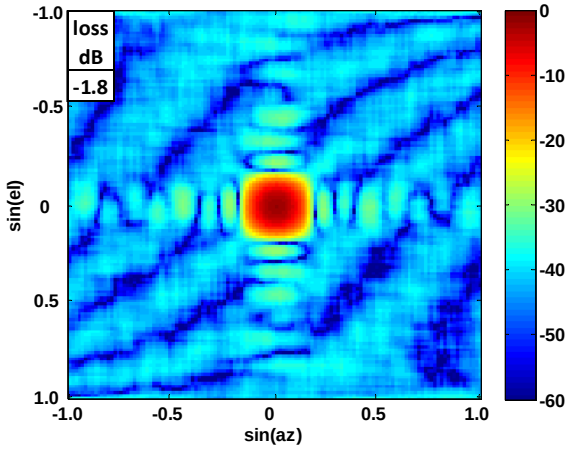

Fig. 10. Uncorrected pattern with two failed elements.

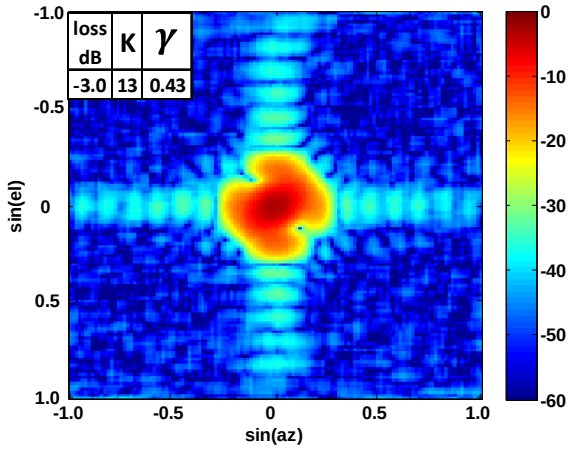

Fig. 11. Corrected pattern with two failed elements.

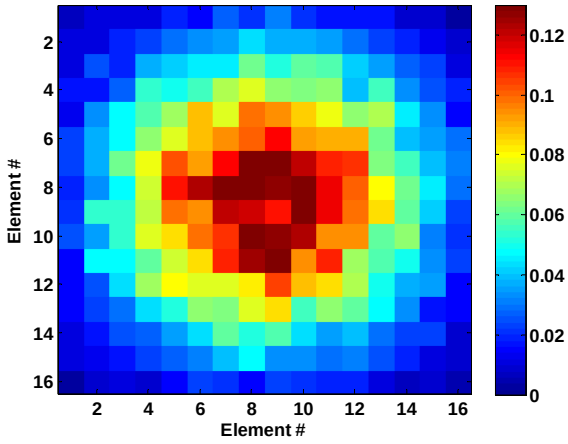

Fig. 12. Beamformer amplitudes with no failed elements.

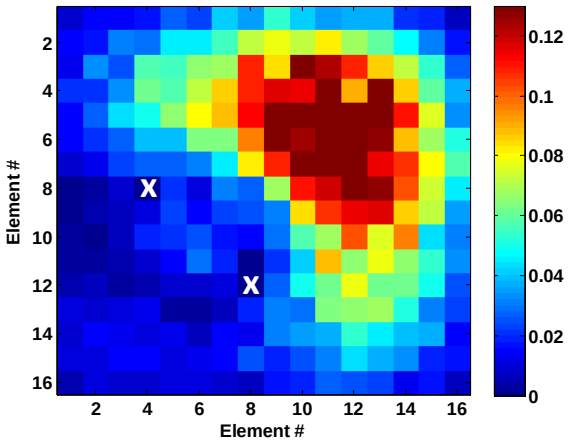

Fig. 13. Beamformer amplitudes with failed elements [8,4] and [12,8].

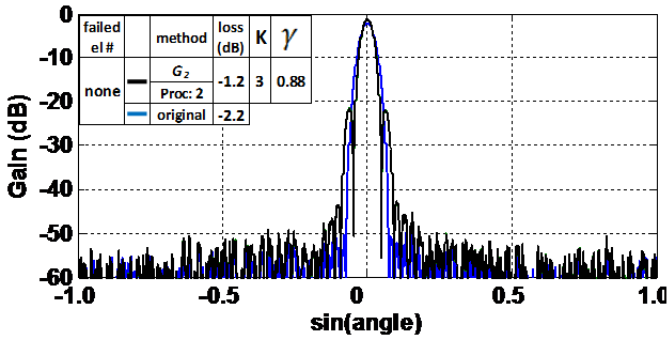

Fig. 14. Antenna patterns with no failed elements and reduced taper loss.